Large Eddy Simulation of liquid metal turbulent mixed convection in a vertical concentric annulus

Luca Marocco*

Department of Energy
Politecnico di Milano
Milan, Italy 20156
Email: luca.marocco@polimi.it

Francesco Garita

Department of Energy
Politecnico di Milano
Milan, Italy 20156

In the present study turbulent forced and mixed convection heat transfer to a liquid metal flowing upwards in a concentric annulus is numerically investigated by means of Large Eddy Simulation (LES). The inner-to-outer radius ratio is 0.5. The Reynolds number based on bulk velocity and hydraulic diameter is 8900, while the Prandtl number is set to a value of 0.026. A uniform and equal heat flux is applied on both walls. LES has been chosen to provide sufficiently accurate results for validating Reynolds-Averaged turbulence models. Moreover, being the thermal sublayer thickness of liquid metals much larger than the viscous hydrodynamic one, liquid metals present a separation between the turbulent thermal and hydrodynamic scales. Thus, with the same grid resolution it is possible to perform a LES for the flow field and a "thermal" Direct Numerical Simulation (DNS) for the temperature field. Comparison of the forced convection results with available DNS simulations shows satisfying agreement. Results for mixed convection are analyzed and the differences with respect to forced convection at the same Reynolds number are thoroughly discussed. Moreover, where possible, a comparison with air is made.

c_p	= specific heat capacity at constant pressure, $J/kg/K$
C_D	= Darcy-Weisbach friction factor
C_f	= Fanning friction factor
g	= acceleration of gravity pointing in negative axial direction, m/s^2
d_h	= hydraulic diameter, m $[d_h = 4\delta]$
Gr_q	= Grashof number $[Gr_q = \frac{\beta g d_h^4 q_w}{\nu^2 \lambda}]$
k	= turbulent kinetic energy, m^2/s^2
L_x	= computational domain extent in streamwise direction, m
N_x, N_r, N_θ	= number of grid points in x, r and θ direction, respectively
Nu	= Nusselt number
P	= pressure, N/m^2
p	= dimensionless dynamic pressure $[p = \frac{P+\rho g x_i \delta_{i1}}{\rho u_b^2}]$
P_k	= shear production of k, m^2/s^3 $[-\overline{u'v'}\frac{\partial \overline{u}}{\partial r}]$
P_Θ	= production of temperature variance, K^2/s $[-\overline{v'\Theta'}\frac{\partial \overline{\Theta}}{\partial r}]$
Pr	= Prandtl number
Pr_t	= turbulent Prandtl number $[Pr_t = \nu_t/\alpha_t]$
q_w	= heat flux at the walls, W/m^2
Re	= Reynolds number $[Re = u_b d_h/\nu]$
R_i, R_o	= wall inner and outer radius, respectively, m
t	= dimensionless time (with u_b and d_h)
T	= temperature, K
T_b	= bulk temperature, K
T_τ	= friction temperature, K $[T_\tau = q_w/\rho c_p u_\tau]$
T_w	= wall temperature, K
u_i	= dimensionless velocity component in i-th direction (with u_b)
u, v, w	= velocity in x,r and θ direction, respectively, m/s
u_b	= bulk velocity, m/s
u_τ	= friction velocity, m/s $[u_\tau = \sqrt{\tau_w/\rho}]$
V	= cell volume, m^3
x_i	= dimensionless i-th cartesian coordinate (with d_h)
x, r, θ	= spatial coordinates in x,r and θ direction, respectively
y	= distance from inner or outer wall, m

*Corresponding author

Special characters

α	= inner-to-outer radius ratio
α_t	= turbulent thermal diffusivity, m^2/s
β	= thermal expansion coefficient, K^{-1}
δ	= half gap width, m [$\delta = 0.5(R_o - R_i)$]
δ_{ij}	= Kronecker delta
Δ	= mean grid size, m
$\Delta x, \Delta y, \Delta\theta$	= grid spacing in x, r and θ direction
ε	= dissipation rate of turbulent kinetic energy, m^2/s^3
η	= Kolmogorov length scale, m [$\eta = (\nu^3/\varepsilon)^{1/4}$]
η_T	= Corrsin length scale, m [$\eta_T = \eta Pr^{-3/4}$]
λ	= thermal conductivity, $W/m/K$
ν	= kinematic viscosity, m^2/s
ν_{SGS}	= subgrid-scale viscosity, m^2/s
ν_t	= turbulent viscosity, m^2/s
ρ	= density, kg/m^3
τ_w	= wall shear stress, N/m^2
Θ	= dimensionless temperature [$\Theta = (T - \overline{T}_b)/(q_w/\rho c_p u_b)$]
Θ^+	= dimensionless temperature [$\Theta = (T - \overline{T}_w)/(q_w/\rho c_p u_\tau)$]

Superscripts and Subscripts

$\overline{(\cdot)}$	= averaged over x,θ and t
$(\cdot)^+$	= normalized by ν, u_τ and T_τ
$(\cdot)'$	= fluctuating component
i	= inner wall
o	= outer wall

1 Introduction

Liquid metals are considered excellent coolant fluids for many engineering applications, e.g. in advanced nuclear reactors [1], as working medium in spallation particle sources [2] and in concentrated solar power research plants [3, 4]. Indeed, they are characterized by a very large molecular conductivity, and consequently by a very low Prandtl number of the order of $10^{-3} \div 10^{-2}$, and by a very high convective heat transfer coefficient. This makes them able to exchange energy more efficiently and with smaller surfaces than conventional fluids. Moreover they remain stable in the liquid phase over a broad range of temperatures. Therefore, they are attractive when the size and weight of the heat exchange devices should be limited and when high thermal loads are present. The underlying physical mechanism of heat transfer in liquid metals significantly differs from that in gases or ordinary liquids. Indeed, the contribution of the molecular thermal conduction to the total heat transfer is much higher for liquid metals than for fluids with a Prandtl number of order one or higher. As a consequence, the results obtained for medium-to-high Prandtl number fluids cannot be directly transferred to liquid metals [5].

The annulus deals as a basis for the analysis of more complex geometries like rod bundles at high pitch-to-diameter ratios, heat exchangers and solar power generators. In contrast to a parallel channel flow or a pipe flow, this geometry presents the additional characteristic of having two walls with a different radius of curvature, thus resulting in asymmetric profiles of all quantities and different friction factors and Nusselt numbers on each wall.

Mixed convection occurs when *forced* convection and *free* convection act simultaneously, i.e. when the fluid motion occurs in response to an externally applied pressure gradient and at the same time to a density variation within the flow. The result is a complex modification of heat transfer performance, due to strong modifications in the structure of turbulence. Depending on flow direction and thermal boundary conditions mixed convection can be classified in *aided* or *opposed*. The first occurs for a vertical upward heated or downward cooled flow, i.e. when the buoyancy forces act in the same direction of the flow. Contrarily, opposed mixed convection occurs for a vertical downward heated or upward cooled flow, i.e. when the buoyancy forces act in the opposite direction to the flow. For an exhaustive and comprehensive description of the phenomenon the interested reader is referred to the works of Ref. [6, 7] and references therein.

The majority of the experimental and numerical studies on mixed convection have been done for air, water or supercritical carbon dioxide, thus for fluids with moderate-to-high Prandtl numbers. Moreover they mainly deal with a flow in a uniformly heated pipe (refer to Ref. [7] and references therein). For low-Prandtl-number fluids such as liquid metals, the number of available literature works significantly drops. As argued in Ref. [7], the reason could be found in the difficulties related to the experimental investigation of these fluids. To the best of the authors' knowledge the most reliable experimental data on mixed convection to liquid metals are still those of Buhr et al. [8] of 1974 for mercury ($Pr = 0.025$) and Jackson et al. [9] of 1994 for sodium ($Pr = 0.005$) flowing in a vertical pipe. From this latter work sodium is found to behave differently from other fluids, including mercury. Indeed, like in laminar flows, heat transfer is enhanced for aided mixed convection and impaired in the opposed case. As stated before, the reason is the high ratio of molecular-to-turbulent thermal diffusivity at least at the investigated Reynolds numbers. On the contrary, mercury seems to behave qualitatively like conventional fluids, i.e. heat transfer is enhanced for opposed turbulent mixed convection and impaired in the aided case. Nevertheless, as shown in the study of Marocco et al. [7], when considering an annulus, even a fluid with a Prandtl number of 0.025 behaves differently from medium-to-high Prandtl number fluids. To the authors' best knowledge the only available studies in literature on turbulent mixed convection of a liquid metal flowing in an annulus are those of Ref. [7] and Ref. [10], the latter for $\alpha = 0.1$ and with only the inner wall heated.

The aim of the present study is to broaden the state-of-the-art general knowledge of turbulent mixed convection to liquid metals and for the annulus in particular. Here only the *aided* case is investigated because of its possible detrimental effect on heat transfer and an inner-to-outer radius ratio of $\alpha = 0.5$ is considered. Large Eddy Simulations are carried out for a constant and uniform heat flux applied on both walls at a Reynolds number of $Re = 8900$ and for a Prandtl number of $Pr = 0.026$, encompassing then among others mercury, gallium-indium-tin and lead-bismuth eutectic, the latter being one of the prominent candidates for "Generation IV" nuclear reactors. At such a Prandtl number the smallest temperature scales are much larger than the corresponding velocity scales [11]. This allows to perform with the same grid resolution a LES for the velocity field and at the same time a "thermal" Direct Numerical Simulation

(DNS) for the temperature field [12]. The adjective "thermal" is added to remark that, even if no heat flux model is used in the temperature equation, its solution is not a true DNS because it depends on the velocity field, which is anyway solved with a subgrid-scale-stress (SGS) model. This hybrid LES/DNS technique can be used to obtain sufficiently accurate results for liquid metal flows with a much coarser grid resolution than required for a full DNS.

2 Governing Equations and Numerical Methodology

For the domain sketched in Fig. 1, the non-dimensional continuity, momentum and energy equations, Eqs. (1) to (3), are solved in cartesian coordinates for an incompressible Newtonian fluid with constant thermophysical properties, no viscous dissipation and with the Boussinesq approximation for buoyancy. All variables are non-dimensionalized by the hydraulic diameter, d_h, and the bulk velocity, u_b. It should be remarked that the velocity and pressure are filtered variables and therefore the subgrid-scale viscosity, ν_{SGS}, appears in the momentum equation. Contrarily, no heat flux model is used for the temperature, which is therefore not a filtered quantity. The last terms on the right-hand side of Eqs. (2) and (3) arise

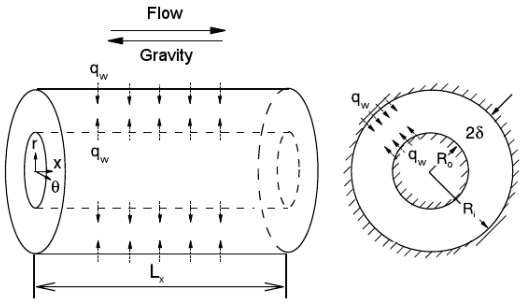

Fig. 1: Schematic of computational domain

from considering a periodic flow in the streamwise direction. Note also that the buoyancy term, i.e. $\Theta\frac{Gr_q}{Re^2}$, in Eq. (2) is only accounted for in the streamwise direction for mixed convection. In Eq. (2), the streamwise pressure gradient (inside the term C_D) is adapted at every time step to satisfy the imposed mass flowrate. The subgrid-scale viscosity, ν_{SGS}, is evaluated with the dynamic Smagorinski-Lilly model described in Ref. [13].

$$\frac{\partial u_i}{\partial x_i} = 0 \tag{1}$$

$$\frac{\partial u_i}{\partial t} + \frac{\partial (u_i u_j)}{\partial x_j} = -\frac{\partial p}{\partial x_i} + \frac{1}{Re}\left(1 + \frac{\nu_{SGS}}{\nu}\right)\frac{\partial^2 u_i}{\partial x_j \partial x_j} + \left(\Theta\frac{Gr_q}{Re^2} + \frac{C_D}{2}\right)\delta_{i1} \tag{2}$$

$$\frac{\partial \Theta}{\partial t} + \frac{\partial (u_i \Theta)}{\partial x_i} = \frac{1}{RePr}\left(\frac{\partial^2 \Theta}{\partial x_i \partial x_i} - 4u_i\delta_{i1}\right) \tag{3}$$

The simulations are performed for a quarter of the full cross-section ($\pi/2$) with the open source code OpenFOAM. The Reynolds number based on bulk velocity and hydraulic diameter is $Re = 8900$ and the Prandtl number $Pr = 0.026$. An inner-to-outer radius ratio of $\alpha = 0.5$ is considered. The pressure-velocity coupling is accomplished through the PIMPLE algorithm (merged PISO-SIMPLE [14]). The momentum and energy equations are integrated in time with a second-order implicit scheme. All terms in the governing equations are discretized with a central differencing scheme. No-slip boundary condition and constant equal uniform heat flux are enforced at the walls. Periodic boundary conditions for velocity and temperature are applied in streamwise and circumferential directions. The domain extent in axial direction is $L_x = 25\delta$ for forced convection and $L_x = 40\delta$ for mixed convection. The adequacy of this choice is discussed later on. The mesh is uniform in streamwise and circumferential directions. In order to capture the sharp velocity gradients, a non-uniform spacing is used in radial direction with the control volumes clustered towards the walls. The distance of the k-th node from each wall until the center of the annular gap can be calculated as follows:

$$\frac{y_k}{\delta} = \frac{1 - r^k}{1 - r^{N_r}} \tag{4}$$

In the above equation the expansion ratio is $r = SF^{1/(1-N_r)}$. The stretching factor, SF, expresses the ratio between the last and first cell width. In this work a value of $SF = 40$ is used. For all simulations a variable time step is used by imposing a maximum CFL (Courant-Friedrichs-Lewy) value of 0.3. This results in a mean computational time step for the coarse/fine grid of 0.038/0.030 δ/u_b and 0.045/0.035 δ/u_b for forced and mixed convection, respectively. Upon reaching a statistically steady condition, the statistics are gathered over a total computational time of 1000 δ/u_b and 1600 δ/u_b for forced and mixed convection, respectively, corresponding to 40 domain wash-throughs.

3 Results

Before proceeding to solve the turbulent mixed convection, the accuracy and reliability of the present numerical simulations are tested by comparing the results obtained for turbulent forced convection with the DNS ones of Ref. [15]. The latter work is done for a fluid having $Pr = 0.71$ and thus only the data of the flow field are compared with the present ones. Actually, the DNS of Ref. [16] is for a fluid with $Pr = 0.026$ at the same Reynolds number of the present investigation, but for a radius ratio of $\alpha = 0.1$. It should be remarked that the reference DNS data from Ref. [15] are not available as electronic database but have been digitalized from the electronic paper. All LES simulations are done for two grids, differing in the number of control volumes in circumferential direction. Indeed, results are known to be quite sensitive to this parameter.

For mixed convection, the works of Ref. [7] and Ref. [10] cannot be used for comparison of the present LES results because both are for higher Reynolds numbers. Moreover, the first uses RANS models, while the second is for $\alpha = 0.1$. Anyway, the validation of the forced convection simulations with DNS data allows to consider also the results for mixed convection as trustworthy, as explained later on in Section 3.2.

3.1 Forced Convection

Table 1 summarizes the resolution for the two different grids used in the simulations together with the reference DNS one from Ref. [15].

	DNS [15]	LES1	LES2
(N_r, N_θ, N_x)	(65,128,320)	(72,24,64)	(72,48,64)
Δy^+_{min}	0.13	0.184	0.191
Δy^+_{max}	12.89	14.77	15.28
$(R_i \Delta\theta)^+$	3.73	18.89	9.77
$(R_o \Delta\theta)^+$	7.10	37.78	19.55
Δx^+	14.23	56.40	58.34

Table 1: Grid resolution normalized with $u_{\tau,i}$ and ν

Both grids are for "wall-resolved" LES, in the sense that they have a DNS-like wall normal resolution. The grid resolution of LES1 is very similar to the one used by Liu et al. [17] for a slightly higher Reynolds number. The latter authors consider it to be adequate but the validation is only made against few experimental data of root mean square velocity fluctuations and surprisingly not against, at that time already available, exhaustive DNS data of Ref. [15]. In order to check the mesh adequacy, we also use a grid (LES2) with twice the control volumes in circumferential direction.

Table 2 lists the values obtained with both grids for the position of maximum streamwise velocity, zero Reynolds stress and for the skin friction coefficient and the Nusselt number on the inner and outer wall, together with the DNS data of Ref. [15] and the data from the correlation of Ref. [18] for Nu. The results of C_f for LES1 strongly differ from the DNS values, while a good agreement is obtained for LES2. Unfortunately the calculated skin friction factor values are not available in Ref. [17], but from the present results it can be argued that the circumferential grid resolution used in that study is not fine enough to correctly capture the sharp velocity gradients at the walls, especially at the outer surface.

In order to investigate it further, the dimensionless velocity and shear stresses are shown in Fig. 2 and Fig. 3, respectively, while the root mean square profiles of the velocity fluctuations in Figs. 4a and 4b. Also here the better agreement between DNS data and LES2 is evident, apart for the root mean square of the circumferential velocity fluctuations, where LES1 seems to perform better. Anyway, the values for both grids in radial and circumferential directions are practically identical. Accordingly, for the thermal field only the results obtained with LES2 will be shown.

	DNS	LES1	LES2	Δ%
$(y/\delta)_{max}$	0.89	0.949	0.949	6.2 / 6.2
$(y/\delta)_0$	0.88	0.983	0.913	10.47/3.61
C_f (inner)	0.00941	0.008506	0.009010	9.6 / 4.25
C_f (outer)	0.00849	0.006044	0.007568	28.8 / 10.8
Nu (inner)	18.10*	16.31	16.69	10 / 7.8
Nu (outer)	8.36*	8.09	8.35	3.3 / 0

Table 2: Position of maximum streamwise velocity, $(y/\delta)_{max}$, and zero turbulent shear stress, $(y/\delta)_0$, Nusselt number and skin friction factor. Values with * calculated with correlation of Ref. [18]

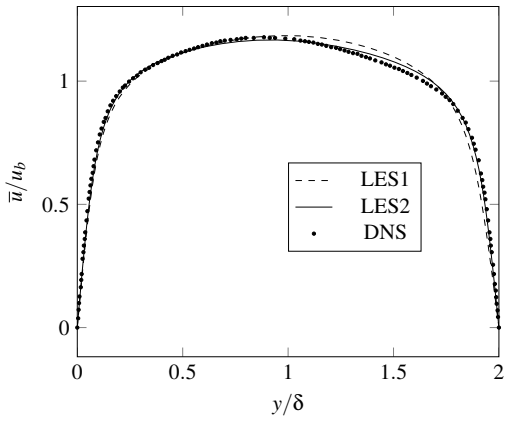

Fig. 2: Mean velocity profiles

When considering the thermal field it is interesting to analyze the relative contribution of the molecular and turbulent heat flux to the total heat flux, as shown in Fig. 5a for a fluid with $Pr = 0.026$ and in Fig. 5b for air. The latter simulation has also been performed by the present authors using the same grid as for LES2 but with a heat flux model also in the temperature equation and considering a subgrid-scale turbulent Prandtl number of 0.45, as suggested by Ref. [11]

It is immediately evident that for air, already at this low Reynolds number, the turbulent heat flux mainly contributes to the total heat flux almost over the entire section. For a low-Prandtl number fluid it is exactly the opposite and the total heat flux practically coincides with the molecular one. This explains, together with the quite similar velocity profiles, the small differences in the Nu number values between LES1 and LES2.

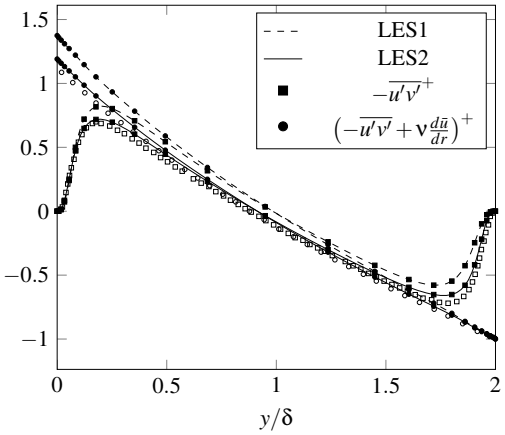

Fig. 3: Turbulent and total shear stress; open symbols refer to DNS of Ref. [15]. Values non-dimensionalized with $u_{\tau,o}$

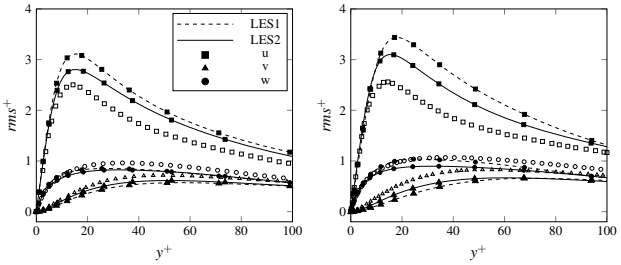

(a) (b)

Fig. 4: Root mean square profiles (rms) of velocity fluctuations; a) inner b) outer; open symbols refer to DNS of Ref. [15]

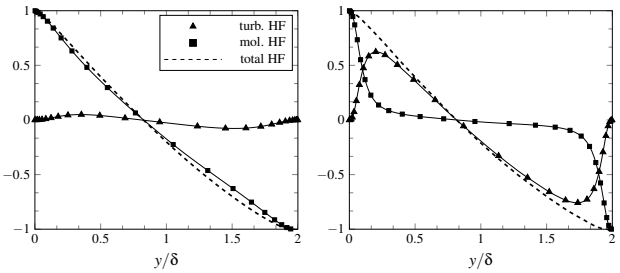

(a) (b)

Fig. 5: Profiles of molecular $(Pr^{-1}d\bar{\Theta}/dr)^+$, turbulent $\overline{(v'\Theta')}^+$ and total $\left((Pr^{-1}d\bar{\Theta}/dr)-\overline{(v'\Theta')}\right)^+$ wall-normal heat flux; a) $Pr = 0.026$ b) $Pr = 0.71$

3.2 Mixed Convection

As suggested by Ref. [7], the buoyancy number defined in Eq. (5) is used to characterize the relative strength of the buoyancy forces.

$$Bo = 8 \cdot 10^4 \frac{Gr_q}{Re^{3.425} Pr^{0.8}} \tag{5}$$

As stated in Ref. [7], the area-weighted wall heat flux is used in the definition of Gr_q. Anyway, for equal values of q_w, as in the present case, the area-weighted averaged value coincides with that on each wall.

In the present work simulations are performed for $Bo = 1.3$, corresponding approximately to the condition of maximum heat transfer impairment. This value has been previously determined with RANS simulations according to the numerical setup described in Ref. [7].

Contrarily to forced convection, for mixed convection there are no available experimental or highly accurate numerical data to compare the results with. Anyway, LES2 performs well for forced convection. Because we simulate the case of maximum heat transfer impairment and thus minimum turbulence intensity, it can be assumed that the same number of control volume elements and wall clustering of LES2 are adequate also for this mixed convection case. The grid resolution for mixed convection differs only slightly from that of forced convection listed in Table 1. Because a longer domain is here used, the number of control volumes in streamwise direction is 102 instead of 64. For the sake of completeness, the simulations are also performed with the coarser grid of LES1. The ratios between C_f and Nu to the corresponding forced convective values obtained with LES2 are summarized in Table 3.

	LES1	LES2
C_f/C_{f0} (inner)	0.798	0.850
C_f/C_{f0} (outer)	0.947	0.992
Nu/Nu_0 (inner)	0.895	0.925
Nu/Nu_0 (outer)	1.030	1.034

Table 3: Mixed-to-forced friction factor and Nusselt number ratios for mixed convection at $Bo = 1.3$. C_{f0} and Nu_0 refer to the forced convection values of LES2

For forced convection the results in terms of Nu obtained with the coarse (LES1) and fine grid (LES2) are practically the same because at this low Re number the turbulent contribution to the total heat flux is negligible and does not affect the temperature field. The same consideration also holds in the case of mixed convection, as shown by the values in Table 3. By contrast, the flow field is much more sensitive to the turbulence intensity. Indeed, the C_f values of forced convection obtained with LES1 strongly differ from those of LES2, which on the other hand are in good agreement with the DNS data. For mixed convection the differences in the C_f values obtained with LES1 and LES2 are much smaller. The reason lies in the reduced level of turbulence at this Bo number, which consequently allows to use a coarser grid resolution. For the sake of clarity, in what follows only the results from LES2 are shown.

Fig. 6 shows the streamwise velocity profile for mixed

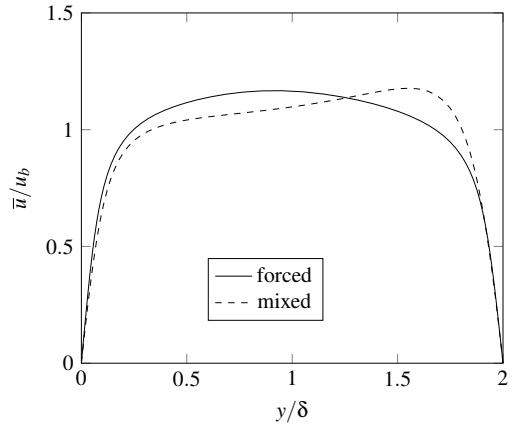

Fig. 6: Mixed and forced convection mean streamwise velocity profiles in global coordinates

convection together with that obtained for forced convection. The former is strongly modified with respect to the forced convection one. For the same wall heat flux, more energy is introduced into the flow at the outer wall, being its surface area bigger than the inner one. The fluid is therefore accelerated close to the outer wall. To preserve a constant mass flowrate, the velocity decreases over the rest of the section. The velocity decrease is more pronounced towards the inner wall because it compensates for the smaller radii.

The streamwise velocity is also plotted in wall units in Fig. 7, together with the DNS data of Ref. [15].

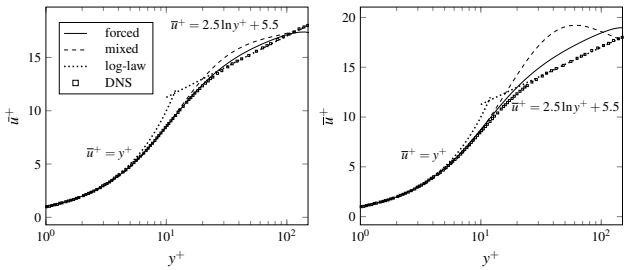

Fig. 7: Mean velocity profile a) inner wall; b) outer wall

The DNS data perfectly fit the log-law of the wall, while the forced convection data from LES2 show some discrepancies, mainly in the outer region. The reason are the different friction factor values between LES2 and DNS and thus the different friction velocities used to normalize the streamwise velocity, as shown in Table 1. For mixed convection the deviation from the log-law is evident and is much more pronounced in the outer region (Fig. 7b).

In order to better understand the values obtained for the mixed-to-forced friction factor ratios in Table 3, the Reynolds shear stresses shown in Fig. 8 should also be considered. Indeed, there is a *direct* effect of buoyancy on the mean velocity and an *indirect* effect on the velocity fluctuations and thus on the turbulence intensity. This can be recognized on the outer wall, where the steeper velocity gradients resulting from the accelerated flow (Fig. 6) are compensated by the reduction of turbulent shear stress (Fig. 8), resulting in practically the same C_f value as for forced convection. On the inner wall the velocity decreases and so does the Reynolds shear stress. Consequently, the friction factor for mixed convection is lower than the corresponding one for forced convection.

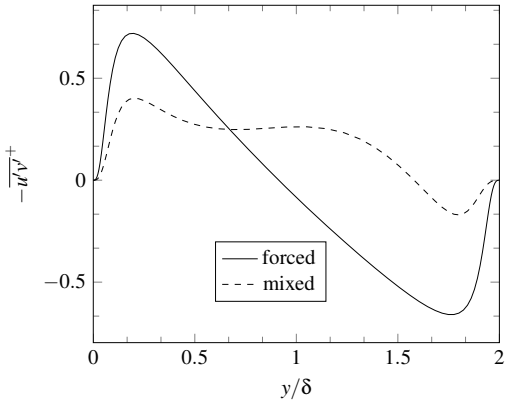

Fig. 8: Mixed and forced convection Reynolds shear stress; Values non-dimensionalized with $u_{\tau,o}$

It is also interesting to analyze the differences in the profiles of turbulent kinetic energy due to buoyancy, shown in Fig. 9a, together with the corresponding profiles of shear production of k, shown in Fig. 9b.

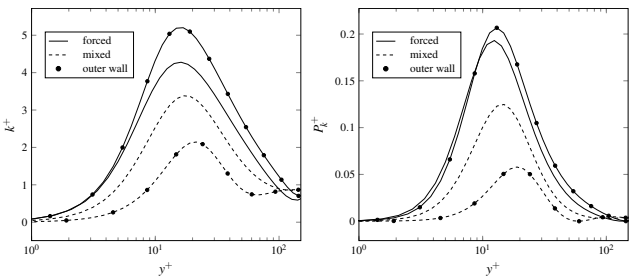

Fig. 9: Profiles of a) turbulent kinetic energy, k; b) shear production of k, P_k

For forced convection the turbulent kinetic energy is higher on the outer wall and the peaks in both inner and outer region are found approximately at the same position. The corresponding production terms of k are almost of the same magnitude and the peaks at the same positions, corresponding to the peaks of k. For mixed convection, due to turbulence impairment, k decreases in both regions with respect to forced convection and so does also the turbulent production.

Moreover, there is an inversion with respect to forced convection, in the sense that now k is much higher in the inner region. The reason is the higher heat rate entering the fluid from the outer wall, implying a higher turbulence reduction here. Accordingly, also P_k is now higher in the inner region. It should also be noted that the peaks of k and P_k close to the inner wall remain almost at the same position as for forced convection, only at a lower value. Vice versa, the peaks in the outer region shift towards the center of the annulus.

Contrarily to C_f, the Nusselt number modification is only caused by the *direct* effect of buoyancy on the velocity field. Indeed, as shown in Fig. 5, at this Reynolds number the turbulent heat flux is practically negligible compared to the molecular one. The same holds even more for the mixed convection case here considered, where turbulence is further impaired. Therefore, as for laminar mixed convection, the Nusselt number increases on the outer wall, where the higher velocity implies higher temperature gradients. On the inner wall, where the velocity and the temperature gradients decrease, the Nusselt number also decreases. The decrease of Nu on the inner wall is more pronounced than the corresponding increase on the outer wall. Indeed, as explained above, due to continuity, the velocity, and thus the velocity gradients, decrease more when approaching the inner wall in order to compensate for the smaller radii.

Fig. 10a shows the temperature profiles in wall coordinates in the inner and outer region, together with the values calculated with the correlation of Ref. [19] valid for a pipe (for the present annular geometry $d_h/2$ has been used instead of the pipe radius in the correlation of Ref. [19]).

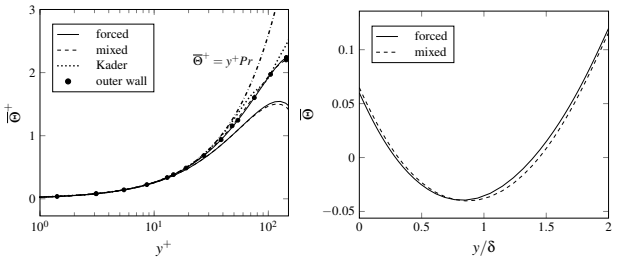

(a) (b)

Fig. 10: Mean temperature a) wall coordinates together with correlation of Ref. [19] for forced convection b) global coordinates

The forced convection temperature profile better agrees with the correlation on the outer region. Indeed, the latter is valid for a pipe (or channel) and the outer wall better approximate this geometry, while the inner temperature field is more influenced by the presence of the other (larger) wall. The discrepancy should reduce by increasing the inner-to-outer radius ratio towards the value of one, corresponding to a parallel plate channel.

The thermal viscous sublayer extends much more towards the core of the annulus compared to the hydrodynamic one, shown in Fig. 7. On the inner wall, where due to the higher curvature the viscous sublayer is thinner, the deviation from the linear viscous profile occurs at $y^+ \approx 25$, while on the outer wall at $y^+ \approx 40$, thus well beyond the hydrodynamic viscous sublayer that ends at approximately $y^+ = 5$. It should be noted that no "log-region" can be recognized in the temperature profiles at this Reynolds number. They resemble more the "transition" region, between viscous and log-region, of the velocity profile. The same conclusion has also been drawn by Ref. [12] for a liquid metal flowing in a channel at a much higher Reynolds number.

The mixed convection temperature profile differs only slightly from the forced one, as can be better recognized from Fig. 10b, where the temperature is plotted in global coordinates. This could sound strange because of the marked differences in the velocity profiles between forced and mixed convection, shown in Fig. 6. The reason is the high molecular conductivity of low-Pr-number fluids, that, at least at this Reynolds number, smears out the differences due to the different velocity fields. Anyway, as discussed previously, the different velocities, and thus advection contributions, close to both walls influence the values of the Nusselt numbers.

Fig. 11 shows the root mean square of the temperature fluctuations and the production of temperature variance on both walls for forced and mixed convection for a liquid metal ($Pr = 0.026$) and only forced convection for air ($Pr = 0.71$). For forced convection, the highest peak is found close to the outer wall, according to the higher heat rate entering the fluid from this surface. The values of Θ'_{rms} for air are much higher than those for liquid metals, indicating the presence of smaller turbulent thermal structures at higher Prandtl numbers. Moreover, the difference between the peaks on the inner and outer wall are lower than for $Pr = 0.026$ and the peaks themselves are more shifted towards the walls.

For mixed convection, analogously to the turbulent kinetic energy and its production due to shear, the values of temperature fluctuations and the production of temperature variance decrease. While for forced convection the position of the peaks of Θ'_{rms} and P_Θ close to both walls almost coincide, for mixed convection the outer peaks are shifted towards the center of the annulus. Moreover, now the peaks close to the inner and outer wall are of practically equal magnitude, while for k the peak close to the outer wall is much lower than that close to the inner one (Fig. 9a). The reason can be found in the similar values of P_Θ. Actually, the outer peak of P_Θ is lower than the corresponding one close to the inner wall even though the peak values of Θ'_{rms} are practically the same. This happens because the dissipation of temperature variance on the outer wall reduces more than that on the inner wall. This compensates for the lower value of P_Θ.

It should also be noted that the values of Θ'_{rms} on the walls differ from zero because of the imposed isoflux boundary condition.

The near-wall behavior of the turbulent viscosity and turbulent thermal diffusivity is shown in Fig. 12.

For the isoflux boundary conditions of the present work, ν_t is proportional to y^3 and α_t to y^2, as also shown in Ref. [15]. For forced convection the profiles for the inner and outer wall

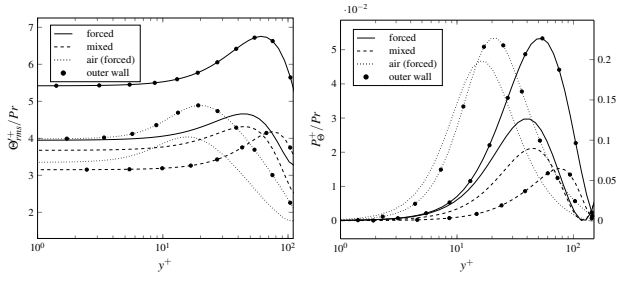

(a) (b)

Fig. 11: Profiles of a) root mean square of temperature fluctuations; b) production of temperature variance, P_Θ (Note that the values of P_Θ for air are plotted on the right axis)

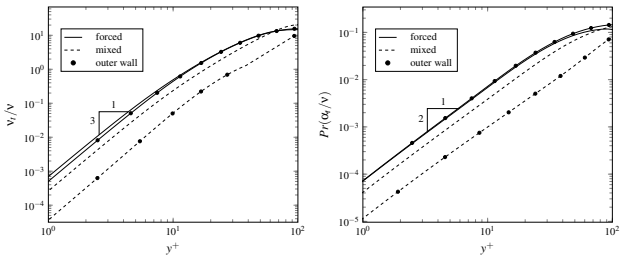

(a) (b)

Fig. 12: Near-wall behavior of a) turbulent viscosity; b) turbulent thermal diffusivity

practically coincide. For mixed convection the profiles on the inner wall are only slightly lower than those for forced convection, while on the outer wall a marked decrease is observed. This highlights once more the higher turbulence reduction in the outer region due to the higher heat rate transferred to the fluid.

In RANS simulations the turbulent heat fluxes are often modeled with the Simple-Gradient-Diffusion-Hypothesis (SGDH), as the product of the temperature gradient and the ratio of turbulent viscosity to turbulent Prandtl number. This approach has also been succesfully used by Ref. [20] to simulate mixed convection to air. As explained in Ref. [7], the assumption of a constant and almost unitary Pr_t does not hold for low-Pr-number fluids. They suggest to use the following correlation proposed by Kays [21] to evaluate Pr_t for mixed convection to a liquid metal:

$$Pr_t = 0.85 + \frac{0.7}{\frac{\nu_t}{\nu} Pr} \tag{6}$$

Fig. 13 shows the calculated Pr_t with LES2 and the corresponding values obtained by inserting the values of ν_t/ν obtained with LES2 in Eq. (6).

The turbulent Prandtl number from the simulations goes to zero approaching the wall because of the asymptotic behavior of ν_t (y^3) and α_t (y^2). Indeed it is defined as $Pr_t = \nu_t/\alpha_t$. Eq. (6) returns very high Pr_t values approaching the walls

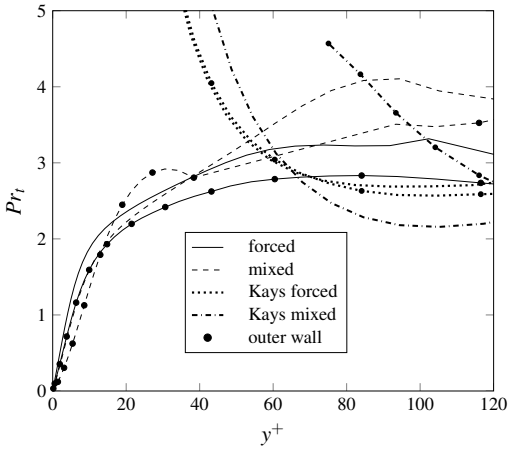

Fig. 13: Turbulent Prandtl number from LES2 and calculated with Eq. (6)

because ν_t/ν tends to zero. This might not be an issue for liquid metals since it implies small turbulent heat flux values in a region where molecular conduction effectively dominates. Indeed, as previously discussed, the thermal viscous sublayer is much thicker than the hydrodynamic one and extends to higher y^+ values.

For forced convection Pr_t attains a "plateau" at approximately $y^+ = 50$. Contrarily to medium-to-high Prandtl number fluids, its value is much higher than unity. Moreover the value in the inner region is higher than that on the outer one because of the higher curvature that results in a higher turbulence intensity and thus in higher values of ν_t (Fig. 12a). The values calculated with Eq. (6) agree quite well with those on the outer region for $y^+ > 60$.

The values of Pr_t obtained for mixed convection in the inner and outer region are higher than the corresponding ones obtained for forced convection, indicating a reduced turbulent energy mixing in this case. In the inner region Pr_t is higher than in the outer one. Contrarily to forced convection, a "plateau" is not so evident anymore. The values calculated with Eq. (6) considerably underestimate Pr_t from the simulations, thus overestimating the turbulent energy mixing.

3.3 Adequacy of computational domain and methodology

Fig. 14 shows the two-point correlations of the streamwise velocity and temperature fluctuations in streamwise and circumferential directions for forced and mixed convection. It should be reminded that the domain extent in streamwise direction differs for the two cases. Indeed, due to the turbulence attenuation more elongated structures are expected to be found for mixed convection and thus a much longer domain in streamwise direction is adopted.

Figs. 14a and 14c show the two-point correlations for the streamwise fluctuating velocity in the streamwise and circumferential direction. The values fall to zero within the separation length, indicating that the chosen domain length is sufficient for the periodic boundary conditions to be ade-

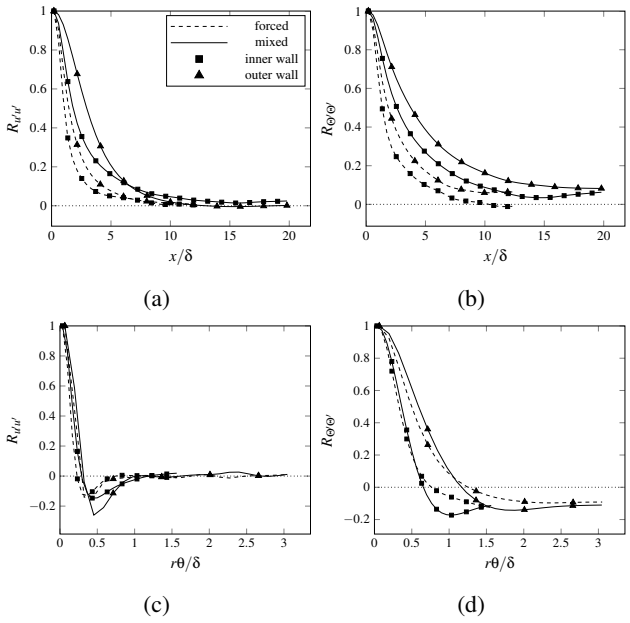

Fig. 14: Two-point correlation coefficients at $y^+ = 5$ from inner and outer wall. a) u' streamwise, b) Θ' streamwise, c) u' circumferential, d) Θ' circumferential

quate for the velocity. As expected, the correlation lengths for mixed convection are greater than for forced convection.

The two-point correlations of the fluctuating temperature in the streamwise direction, shown in Fig. 14b, neither drop to zero for forced nor for mixed convection, indicating that an even larger streamwise domain should be used for both simulations in order to capture the largest thermal structures. These latter are more elongated in streamwise direction for mixed than for forced convection, as recognizable by the bigger integral length scale (area under the curve).

As shown in Fig. 14d, the correlations in circumferential direction do not drop to zero for both forced and mixed convection. This fact does not prevent the use of only one-quarter of the domain in this direction, as done in the present study. Indeed, as reported in Ref. [22], the reason is the use of an isoflux boundary condition at the wall, which implies a non-zero fluctuating temperature on it. As shown in Ref. [23], for forced convection no appreciable differences are found when using the full circumferential domain.

It is important to check *a posteriori* that the adopted mesh resolution actually allows to catch also the smallest scales in the temperature field, thus avoiding to introduce a subgrid heat flux model in the temperature equation. These smallest scales are the Kolmogorov length scale for the velocity field, η, and the Corrsin length scale for the temperature field, $\eta_T = \eta Pr^{-3/4}$. They are calculated with the dissipation rate of turbulent kinetic energy obtained with the present simulations. To completely resolve the temperature field the mean grid size, Δ, calculated as the cubic root of the cell volume, must be such that $\Delta/\eta_T \ll 1$. As shown in Fig. 15, where η, η_T and Δ are plotted in non-dimensional form, the above criterion is satisfied. At the same time the necessity of a subgrid-scale model in the momentum equation is evident, lying the mean grid size above the Kolmogorov scale.

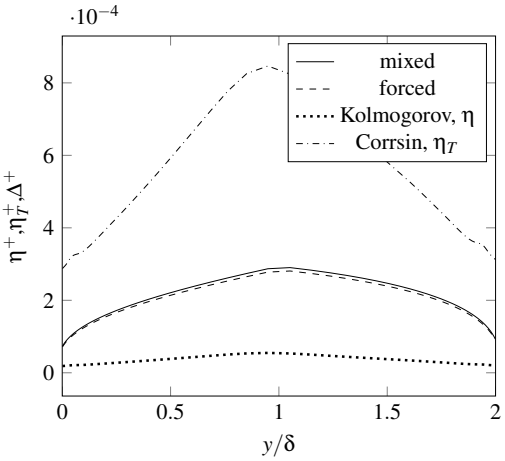

Fig. 15: Kolmogorov scale, Corrsin scale and Δ non-dimensionalized with corresponding mean friction velocity

The separation between hydrodynamic and thermal scales can be also appreciated in the instantaneous visualization of the velocity and temperature fields for forced convection, shown in Fig. 16. Indeed, the temperature field is much smoother than the velocity one, being the thermal smallest structures much larger than the corresponding hydrodynamic ones.

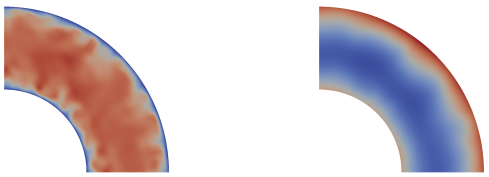

Fig. 16: Visualization of instantaneous a) velocity field b) temperature field

4 Conclusions

In this paper forced and aided mixed convection to a fluid with $Pr = 0.026$ and at $Re = 8900$ flowing in a uniformly heated annulus is simulated with a hybrid LES/DNS methodology, in the sense that with the same grid a LES for the velocity field and a DNS for the temperature field is performed. This is allowed for low-Pr-number fluids, for which the smallest thermal scales are much bigger than the corresponding hydrodynamic ones. The validity of this approach is confirmed by the fact that the mean grid scale is larger than the Kolmogorov scale but much smaller than the Corrsin scale.

Two different grids, one having twice as many elements in circumferential direction as the other, are used. For forced convection the results of the finest one are in much better agreement with available DNS data, confirming the sensitivity to the resolution in this direction. Mixed convection is simulated at a buoyancy strength corresponding to approximately the maximum turbulence reduction. This condition has been determined with previous RANS simulations. Both grids return almost the same results. Therefore, when simulating mixed convection in the reduced turbulence intensity regions a grid with a coarser resolution can be used.

The friction factor coefficient is directly influenced by buoyancy through the modified velocity field and indirectly through the modified turbulence field. On the other hand, at this low Reynolds and Prandtl number, the Nusselt number is only influenced by the modified velocity field, being the contribution of the turbulent heat flux to the total one negligible. This points to the fact that the Reynolds analogy, implying the same exchange mechanism influencing C_f and Nu, does not apply to mixed convection in general and specifically to liquid metals.

When plotted in wall coordinates, the mixed convection velocity profile deviates substantially from the log-law of the wall in the outer region, while a lower discrepancy is found in the inner region. The temperature profile does not show any log-region at this Prandtl and Reynolds number. Moreover, the thermal viscous sublayer extends much more within the annular cross-section compared to the the hydrodynamic viscous one, highlighting the strong molecular contribution to heat transfer for low-Pr-number fluids. The strong wall-normal conduction also implies quite similar temperature profiles for forced and mixed convection, by smearing out the differences eventually due to the different velocity profiles.

The turbulent Prandtl number, important for thermal RANS simulations based on the Single-Gradient-Diffusion-Hypothesis, is evaluated through a correlation developed for low-Pr-number fluids using the computed turbulent-to-molecular viscosity ratio. It is then compared to the one determined from the simulation results. The agreement is good for forced convection, while for mixed convection the correlation returns too low values. Therefore, at least when dealing with wall bounded attached flows, as that here considered, and provided that the turbulent-to-molecular viscosity ratio is correctly predicted, this correlation can be applied to liquid metals forced convection. For mixed convection it should be used with care, particularly at higher Reynolds numbers, where the turbulent contribution to heat transfer becomes more important and should be then predicted correctly in order to obtain reliable results.

The two-point correlations for the fluctuating temperature in streamwise direction do not drop to zero for the domain lengths of the present study, namely 25δ for forced and 40δ for mixed convection, being δ half the width between inner and outer wall. For mixed convection the values remain higher than for forced. On the one hand this suggests the necessity to use an even larger streamwise domain for both cases and on the other hand it indicates the presence of larger streamwise thermal structures for mixed convection.

Besides the less computational effort for the same Reynolds number, an important advantage of this hybrid LES/DNS approach is the possibility to simulate flows at higher Reynolds numbers, where a full DNS would require a too high computational time. Simulations at high *Re* numbers are important for liquid metals, from the one part to obtain higher turbulent-to-molecular thermal diffusivity ratios and from the other part to provide a database to be used for the validation of RANS turbulence models, that are computationally cheaper and hence still much more attractive to the industry.

References

[1] Pacio, J., Daubner, M., Fellmoser, F., Litfin, K., Marocco, L., Stieglitz, R., Taufall, S., and Wetzel, T., 2014. "Heavy-liquid metal heat transfer experiment in a 19-rod bundle with grid spacers". *Nucl. Eng. Des.,* **273**, pp. 33 – 46.

[2] Litfin, K., Batta, A., Class, A., Wetzel, T., and Stieglitz, R., 2011. "Investigation on heavy liquid metal cooling of {ADS} fuel pin assemblies". *J. Nucl. Mater.,* **415**(3), pp. 425 – 432.

[3] Flesch, J., Fritsch, A., Cammi, G., Marocco, L., Fellmoser, F., Pacio, J., and Wetzel, T., 2015. "Construction of a test facility for demonstration of a liquid lead-bismuth-cooled 10 kw thermal receiver in a solar furnace arrangement - sommer". *Energy Procedia,* **69**, pp. 1259 – 1268.

[4] Marocco, L., Cammi, G., Flesch, J., and Wetzel, T., 2016. "Numerical analysis of a solar tower receiver tube operated with liquid metals". *Int. J. Therm. Sci.,* **105**, pp. 22 – 35.

[5] Pacio, J., Marocco, L., and Wetzel, T., 2015. "Review of data and correlations for turbulent forced convective heat transfer of liquid metals in pipes". *Heat Mass Transfer,* **51**, pp. 153–164.

[6] Jackson, J., Cotton, M., and B.P.Axcell, 1989. "Studies of mixed convection in vertical tubes". *Int. J. Heat Fluid Fl.,* **10**(1), pp. 2–15.

[7] Marocco, L., Alberti di Valmontana, A., and Wetzel, T., 2017. "Numerical investigation of turbulent aided mixed convection of liquid metal flow through a con-

centric annulus". *Int. J. Heat Mass Tran.,* **105**, pp. 479 – 494.

[8] Buhr, H. O., Horsten, E. A., and Carr, A. D., 1974. "The distortion of turbulent velocity and temperature profiles on heating, for mercury in a vertical pipe". *ASME J. Heat Transf.,* **96**(2), pp. 152–158.

[9] Jackson, J., Axcell, B., and Walton, A., 1994. "Mixed convection heat transfer to sodium in a vertical pipe". *Exp. Heat Transfer,* **7**, pp. 71–90.

[10] Marocco, L., Loges, A., Wetzel, T., and Stieglitz, R., 2012. "Experimental investigation of the turbulent heavy liquid metal heat transfer in the thermal entry region of a vertical annulus with constant heat flux on the inner surface". *Int. J. Heat Mass Tran.,* **55**(23-24), pp. 6435 – 6445.

[11] Grötzbach, G., 2013. "Challenges in low-Prandtl number heat transfer simulation and modelling". *Nucl. Eng. Des.*(264), pp. 41–55.

[12] Duponcheel, M., Bricteux, L., Manconi, M., Winckelmans, G., and Bartosiewicz, Y., 2014. "Assessment of RANS and improved near-wall modeling for forced convection at low prandtl numbers based on LES up to $Re_\tau = 2000$". *Int. J. Heat Mass Tran.,* **75**(0), pp. 470 – 482.

[13] Lilly, D., 1992. "A Proposed Modification of the Germano Subgrid-Scale Closure Method". *Physics of Fluids A,* **4**(3), pp. 633–635.

[14] Greenshields, C., 2016. *OpenFOAM User Guide version 4.0*. OpenFOAM Foundation Ltd., June.

[15] Chung, S. Y., Rhee, G. H., and Sung, H. J., 2002. "Direct numerical simulation of turbulent concentric annular pipe flow: Part 1: Flow field". *Int. J. Heat Fluid Fl.,* **23**(4), pp. 426 – 440.

[16] Ould-Rouiss, M., Redjem-Saad, L., Lauriat, G., and Mazouz, A., 2010. "Effect of prandtl number on the turbulent thermal field in annular pipe flow". *Int. Commun. Heat Mass,* **37**(8), pp. 958 – 963.

[17] Liu, N., and Lu, X., 2004. "Large eddy simulation of turbulent concentric annular channel flows". *Int. J. Numer. Meth. Fl.,* **45**, pp. 1317–1338.

[18] Kays, W., and Leung, E., 1963. "Heat transfer in annular passages - hydrodynamically developed turbulent flow with arbitrarily prescribed heat flux". *Int. J. Heat Mass Tran.,* **6**(7), pp. 537 – 557.

[19] Kader, B., 1981. "Temperature and concentration profiles in fully turbulent boundary layers". *Int. J. Heat Mass Tran.,* **24**(9), pp. 1541 – 1544.

[20] Kim, W., He, S., and Jackson, J., 2008. "Assessment by comparison with DNS data of turbulence models used in simulations of mixed convection". *Int. J. Heat Mass Tran.,* **51**(56), pp. 1293 – 1312.

[21] Kays, W., 1994. "Turbulent Prandtl number - Where are we?". *ASME J. Heat Transfer,* **116**(2), pp. 284–295.

[22] Tiselj, I., 2014. "Tracking of large-scale structures in turbulent channel with direct numerical simulation of low prandtl number passive scalar". *Physics of Fluids,* **26**, p. 12511.

[23] Garita, F., 2017. "Large eddy simulation of turbulent forced and mixed convection to a liquid metal flowing in an annulus". Master's thesis, Politecnico di Milano.